Template-Free and Seedless Growth of Pt Nanocolumns: Imaging and Probing Their Nanoelectrical Properties

Raffaella Lo Nigro,[†,*] Graziella Malandrino,[‡,*] Patrick Fiorenza,[†] and Ignazio L. Fragalà[‡]

[†]Istituto per la Microelettronica e Microsistemi, IMM-CNR Stradale Primosole 50, 95121 Catania, Italy, and [‡]Dipartimento di Scienze Chimiche, Università di Catania, and INSTM, UdR Catania, v.le A. Doria 6, 95125 Catania, Italy

ABSTRACT The electrical conductivity of platinum nanocolumns has been imaged and measured by conductive atomic force microscopy. The successful syntheses of well-aligned ⟨100⟩-oriented Pt nanocolumns on both random and oriented substrates have been carried out *via* a simple and seedless metal–organic chemical vapor deposition process. Control of the crystalline quality has been achieved by carefully selecting operational conditions. The growth mechanism, depending on deposition parameters (including deposition temperature, oxygen partial pressures, deposition time, and substrate nature), has been examined in detail.

KEYWORDS: nanocolumns · platinum · MOCVD · electrical characterization

As a consequence of the increasing miniaturization of electronic and magnetic devices, nanostructured materials are receiving more and more attention, especially due to their optical, electrical, and mechanical properties, which differ definitively from those of bulk materials.[1–3] Thus, in the emerging field of nanoscience and nanotechnology, nanotubes, nanorods, and nanowires are key forms for both understanding the properties of nanostructures and developing new nanodevices.[4–8] Several strategies have been developed for the growth of nanostructured materials. Known methods,[9–18] however, require high temperatures and special conditions; in some cases, they result in complex and tedious procedures. For instance, the selection of suitable catalysts and templates is not straightforward, and the removal of templates and/or the stabilization of unsupported nanostructures in some cases represent crucial issues that may compromise the structural and physical properties.[19] Metal–organic chemical vapor deposition (MOCVD) procedures offer, in the case of nanomaterials, the usual advantages associated with easy deposition over large areas, as required in many advanced technological and industrial applications.

Platinum nanostructures, in particular, are expected to be important components in future nano-electronics, due to their interesting properties that include a very high chemical stability, a strong resistance to oxidation, and a remarkable thermal conductivity. Because of these properties, much attention has been devoted to the study of Pt films, which are used as electrical contacts in semiconductor devices,[20,21] protective coatings for special instruments,[22] and catalytic agents in different chemical processes.[23–25] Nevertheless, the scaling-down of electronic circuits will soon need nanostructured platinum materials; hence, experimental methods suited for directly addressing the electrical properties of platinum nanostructures are highly desirable.

To date, Pt films have been grown by different techniques, including molecular beam epitaxy (MBE),[26,27] pulsed laser deposition,[28,29] sputtering,[30,31] and MOCVD.[32–37] In particular, various complexes have been tested as platinum MOCVD precursors, such as [(η^5-Cp)$PtMe_3$],[38] [(η^5-MeCp)$PtMe_3$],[38,39] alkylplatinum complexes of the types [$PtMe_2L_2$] and [$PtR(Me)L_2$],[40] and bis(acetylacetonato)platinum(II).[41,42]

On the other hand, the growth of Pt nanostructures has been achieved mainly by template synthetic methods.[43–46]

In this paper, we report on a seedless and template-free MOCVD approach to the synthesis of Pt nanocolumns. Uniform arrays have been obtained on large-area substrates having different natures (glass, Ni-based alloy, namely Hastelloy C276, and $SrTiO_3$(100) single crystals). Here, we illustrate the principle behind this synthetic approach by studying both the role of individual operational parameters in the process and the influence of these parameters on the morphologies of Pt samples. In

*Address correspondence to raffaella.lonigro@imm.cnr.it, gmalandrino@dipchi.unict.it.

Received for review June 20, 2007 and accepted September 20, 2007.

Published online October 5, 2007.
10.1021/nn700068u CCC: $37.00

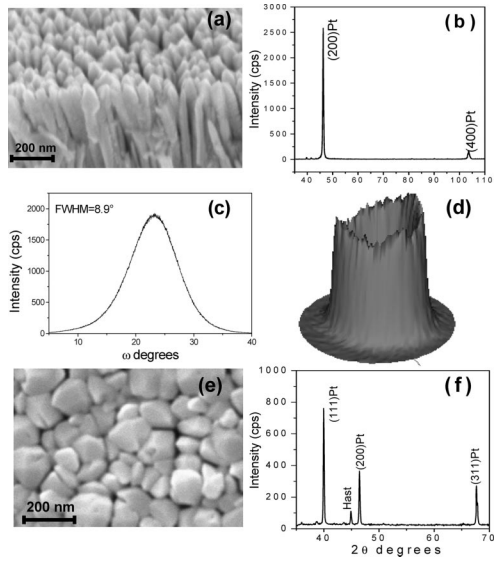

Figure 1. (a) Typical SEM image of Pt nanocolumns grown in the 280–400 °C range on glass substrate without template and/or seeds. (b) Typical XRD pattern of ⟨100⟩-oriented Pt samples grown in the 280–400 °C deposition temperature range. (c) Rocking curve of the ⟨100⟩ Pt nanocolumns recorded using the 200 reflection. (d) Pole figure of the Pt nanocolumns recorded using the 111 reflection. (e) SEM image of a Pt film grown at 450 °C. (f) XRD pattern of a polycrystalline Pt sample grown at deposition temperature >400 °C.

addition, the study of the electrical properties at the nanoscale level by conductive atomic force microscopy (C-AFM) is reported. C-AFM provides a direct imaging of the morphology and electrical properties of the platinum nanocolumns and, therefore, offers a clear perception of the low-dimensional physical properties.

RESULTS

The present study describes the growth of ⟨100⟩-oriented platinum nanocolumns on different substrates (glass, Hastelloy C276, and $SrTiO_3$(100)) by MOCVD, using the platinum(II) acetylacetonate ($Pt(acac)_2$) precursor without catalytic or template actions.

First, experiments were carried out on a glass substrate in the 220–550 °C temperature range using flows of 100 sccm Ar and 200 sccm O_2. This substrate was chosen on the basis of several considerations: (i) it is amorphous, and thus it does not influence the orientation of Pt growth; (ii) it is resistant to oxidation; and (iii) it is chemically stable in the investigated temperature range. The onset of Pt deposition was observed at 250 °C. However, slightly higher deposition temperatures (280 °C) were required to obtain a better homogeneity over the entire 10 × 10 mm^2 substrate area.

In the 250–400 °C range, Pt nanocolumns were obtained (Figure 1a). The related X-ray diffraction (XRD) patterns (Figure 1b) show only two peaks, centered at $2\theta = 46.2°$ and 103.65°, related to 200 and 400 platinum reflections, respectively. This is indicative of textured nanostructures along the ⟨100⟩ direction.

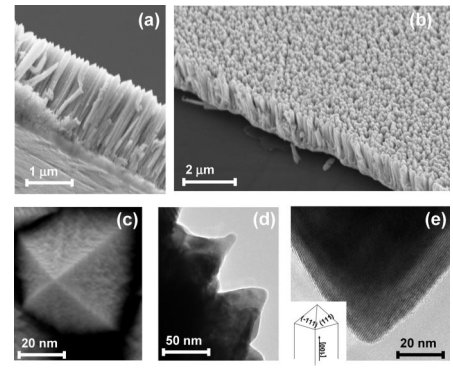

Figure 2. (a) SEM cross-section image of the Pt nanocolumns perfectly perpendicular to the substrate surface. (b) SEM top view showing the homogeneous growth of the Pt nanocolumns on the substrate, which was completely covered. (c) SEM magnification of the Pt nanocolumn tip, consisting of four triangular {111} facet faces. (d) TEM cross-section image of Pt nanocolumns, showing that Pt tips are sharp and 20 nm wide. (e) High-resolution TEM image of the nanocolumn tip, indicating that the four triangular top faces possess a lattice space of 0.227 nm, related to the d_{111} space of cubic Pt, as modeled in the inset.

The related rocking curves (Figure 1c), recorded using the 200 reflection, display full width at half-maximum (fwhm) values ranging from 9.8° to 8.5°. These values, even though much greater than those obtained for epitaxial films on single-crystal substrates, provide clear evidence that oriented Pt nanoarrays can be easily obtained on random substrates using a catalyst-free and template-free MOCVD approach. Better insight into the in-plane orientation has been obtained from the pole figure shown in Figure 1d. Pole figures were recorded using the 111 reflection ($2\theta = 39.90°$) as a pole. All the present samples grown in the 250–400 °C range show a circular feature, obtained at $\Psi = 54°$, as a consequence of there being no in-plane texturing. Conversely, in-plane-oriented samples would have shown four peaks repeated every 90° of φ.

In the case of depositions beyond 400 °C, the data collected pointed out that the samples are mainly random polycrystals, as demonstrated by the related XRD patterns (Figure 1f), which show all the reflections expected for a polycrystalline Pt sample (JCPDS No. 4-0802). Scanning electron microscopy (SEM) images (Figure 1e) of samples deposited at higher T_{dep} show a quite different morphology. There is no evidence of nanocolumn formation, but rounded grains 200 nm wide are observed. This is a convincing indication that the nanostructure critically depends on deposition temperature.

A cross-sectional SEM image (Figure 2a) of samples grown at 250–400 °C suggests that Pt nanocolumns grow almost perfectly vertical to the substrate surface. A typical MOCVD deposition (60 min) yielded columns with diameters ranging between 40 and 80 nm and lengths of 1.8–2 μm, so that the aspect ratio ranges from 22.5 to 50. The average size increases with longer deposition times, up to 100–150 nm in width and 8 μm

length for 3 h experiments. In every case, note that the substrate is uniformly covered (Figure 2b). Thus, the presently reported approach can be an appealing method for the growth of nanostructured arrangements on very large areas.

Each nanocolumn grows along the ⟨100⟩ direction and is capped by pyramids, the four triangular faces of which are clearly visible in Figure 2c.

Further morphological characterization using transmission electron microscopy (TEM) shows that typical Pt nanocolumns have sharp tips of 20 nm width (Figure 2d). The high-resolution TEM image (Figure 2e) demonstrates that the four triangular top faces possess a lattice space of 0.227 nm. This value is in agreement with the d_{111} interplanar distance of cubic Pt. Thus, the nanocolumns' tips consist of {111} planes which represent the most stable planes in a face-centered-cubic (fcc) system in terms of surface energy.

Finally, the sample purity was evaluated by wavelength-dispersive X-ray (WDX) analysis. In particular, there is no evidence of carbon contamination (<2%) in the entire 250–550 °C range, as expected for clean decomposition processes. This is because oxygen plays a crucial role not only in determining the formation of the nanocolumns (*vide infra*) but also in regard to the purity of the arrays, accordingly to studies previously reported on the deposition of copper oxide films from the $Cu(acac)_2$ precursor.[47,48] In fact, oxygen influences the decomposition of acetylacetonate or other nonfluorinated ligands, helping remove the organic byproducts produced during decomposition.[49,50] In the case of platinum, hydrogen has also been shown to play a key role in reducing the carbon impurities.[51]

Study of Process Parameters. A better understanding of the role played by various deposition parameters in controlling the morphology can be obtained by an accurate comparison among samples deposited under different conditions, *i.e.*, evaluating the influence of the deposition temperature, the sublimation precursor temperature, the oxygen partial pressure, and the nature of the substrate.

In regard to the effect of the deposition temperature, several experiments were carried out in the 250–550 °C range, keeping constant the Ar flow (100 sccm), the oxygen flow (200 sccm), and the sublimation temperature (170 °C).

The Arrhenius log plot of deposition rate vs $1/T$ (Figure 3a) shows, over the entire temperature range, the profile typically associated with CVD processes. In the lower T_{dep} region (250 °C < T_{dep} < 380 °C) a linear trend is observed, indicating that the deposition occurs under a kinetically controlled regime. Fitting the experimental data in the linear range (250 °C < T_{dep} < 380 °C) provides an apparent activation energy for the process of 23 ± 2 kJ mol^{-1}.

Upon increasing T_{dep} to 380–450 °C, the deposition rate no longer depends on the temperature. Therefore, the growth rate is limited by mass transport of the precursor to the substrate surface. Under this regime, the maximum growth rate is 33.3 nm/min. Beyond 450 °C, the deposition rate decreases due to the depletion wall effect.

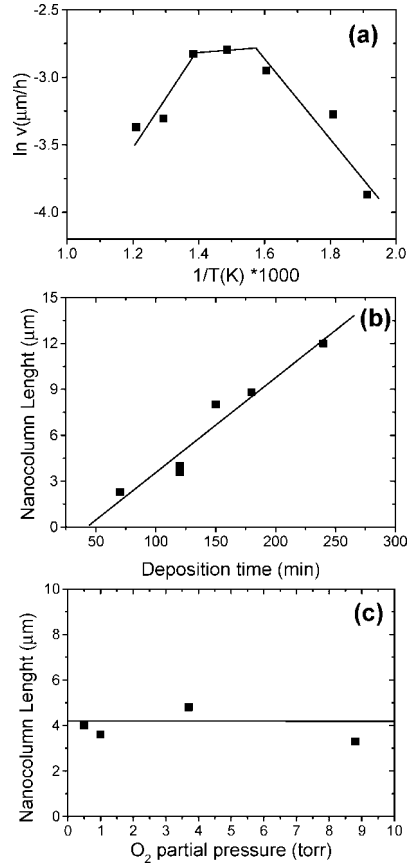

Figure 3. (a) Growth rate of Pt samples *vs* $1/T_{dep}$ in the 250–550 °C range. (b) Plot of the nanocolumn length *vs* deposition time at T_{dep} = 280 °C, showing a linear trend. (c) Pt nanocolumn length *vs* oxygen partial pressure from 1 to 8.8 Torr.

Finally, at T_{dep} = 280 °C, usually adopted for standard experiments, the nanocolumn length depends linearly upon the deposition time (Figure 3b).

Influence of Sublimation Rate of the Pt Source and Influence of Oxygen Partial Pressure. In these experiments, the deposition temperature was kept constant at 280 °C, the Ar flow was maintained at 100 sccm, and the oxygen flow was maintained at 200 sccm. The precursor sublimation temperature was varied in the 150–180 °C range.

Clearly, fiber texturing and surface morphology do not depend on the precursor sublimation T in the 150–170 °C range, while higher sublimation T (180 °C) causes the formation of some larger nanocolumns (>100 nm wide) with a less uniform size distribution. Therefore, it can be concluded that precursor temperature mainly controls the size distribution and does not affect the texturing.

The influence of oxygen partial pressure (0.5–8.8 Torr) was investigated by varying the oxygen flow from 50 to 800 sccm. The experiments were carried out at

280 °C, using a sublimation temperature of 170 °C and an Ar flow of 100 sccm.

It was observed that low oxygen partial pressure (0.5 Torr) yields poorly crystalline samples. In contrast, greater oxygen partial pressures (≥1 Torr) favor the ⟨100⟩ orientation, and the related XRD patterns, in fact, show more intense and narrower 200 peak intensity, indicating a better crystallinity.

There is evidence that $P_{O_2} > 1$ Torr is of relevance since experiments carried out in the absence of oxygen and using an additional Ar flow did not result in the formation of platinum nanocolumns. Moreover, further experiments adopting a delayed O_2 flow (introduced after 30 min) resulted in the sudden growth of platinum nanocolumns (observable by the "naked eye" in the form of a black coating of the substrate) just after the O_2 feeding.

The oxygen partial pressure, however, has no influence on the growth rate (Figure 3c); in fact, no change in the Pt nanocolumn length was observed by varying P_{O_2} from 1 to 8.8 Torr.

In addition, the influence of oxygen flow on the Pt nanocolumn size is negligible. However, it plays a crucial role in determining the ⟨100⟩-oriented growth mode, and it assures the preparation of pure and C-free samples.

Influence of Substrate Nature. To test the influence of the nature of the substrate, several further experiments were carried out at 280 °C on both random and single-crystal substrates. In particular, Hastelloy C276 (Ni-based alloy) foils were used as random metallic substrates, while $SrTiO_3$(100) was employed to test the effect of an oriented single-crystal substrate.

Platinum samples deposited on Hastelloy C276 consist of ⟨100⟩-oriented Pt nanocolumns (Figure 4a), similar to samples deposited on glass. Thus, amorphous and metallic substrates allow the growth of platinum ⟨100⟩-oriented nanocolumns.

The influence of an oriented single-crystal substrate, namely $SrTiO_3$(100), was tested as well. In this case, the chosen lattice parameter ($a = 3.905$ Å) is very close to that of platinum ($a = 3.923$ Å). In principle, epitaxial Pt films were expected due to the very small lattice mismatch (0.45%). Nevertheless, platinum samples deposited on $SrTiO_3$(100) substrates in the range 250−400 °C showed the same texturing and morphology observed in the case of random substrates (Figure 4b). No improvement of the *c*-axis alignment of the nanocolumns was observed, and the fwhm values (8°) of the rocking curves are close to those found on glass. Moreover, Pt samples deposited above 400 °C, up to 850 °C, are polycrystalline and do not possess the columnar morphology; instead, square ordered grains are clearly visible in Figure 4c.

In conclusion, the present low-temperature MOCVD process appears to be substrate-independent and produces high-quality nanocolumns on glass, Hastelloy C276 alloy, and $SrTiO_3$(100) single crystals. In particular, our studies indicate that morphological and structural properties are closely related to the temperature range adopted in the deposition process.

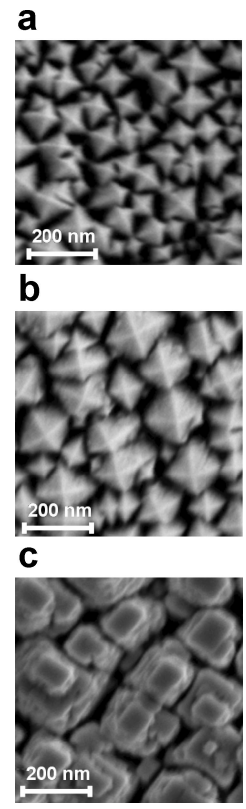

Figure 4. SEM images of the surface morphology of Pt samples grown (a) at 280 °C on Hastelloy C276 substrates, (b) at 280 °C on $SrTiO_3$(100)-oriented substrates, and (c) on $SrTiO_3$(100) substrate above 450 °C.

C-AFM Measurements. The electrical properties of the Pt nanocolumns on Hastelloy C276 substrates were investigated by C-AFM measurements, a variant of atomic force microscopy that uses a conductive cantilever tip connected with a pre-amplifier module. C-AFM can, therefore, collect simultaneously both the morphological image and the current map. Alternatively, it is possible to measure a local current *versus* voltage upon stopping the scan.

Preliminary electrical studies on Pt nanocolumns were performed by a simultaneous morphological and current imaging at fixed voltage (+1 V). In the current map (Figure 5, right), preferential routes for the electrical conduction with current peak intensities on top of each single nanocolumn are shown. There is no evidence of notable variations of current transport among different nanocolumns, although some fluctuations occur at the boundaries, the spatial distribution of which can be easily identified due to the abrupt current drop in the corresponding regions. This is an indication of a well-defined barrier at the boundaries among nanocolumns. Conversely, nanocolumns represent separate blocks rather than particularly rough grains (inset of Figure 5).

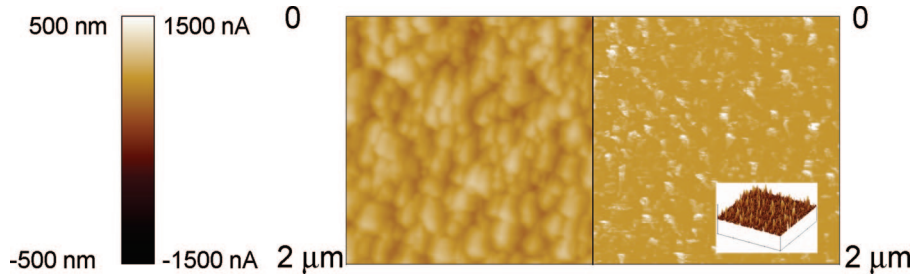

Figure 5. AFM morphological image (left) and the current map (right) of the Pt nanocolumns. The 3-D image of the current map (inset) indicates a well-defined barrier at the boundaries among nanocolumns, which represent blocks rather than particularly rough grains.

Morphological and current imaging at different bias voltages on a nanocolumn area region and on plain Hastelloy C276 were compared as well. Figure 6a shows an edge in the scanned regions at biased different voltages due to the absence of Pt nanocolumns in the left part of the image. The substrate current maps show a constant characteristic with no significant current variation upon increasing the voltage in the considered voltage range (22–32 mV). By contrast, the presence of nanocolumns causes strong current variation upon increasing the tension. This different behavior is highlighted in Figure 6 by the color variation in both regions. In particular, below 25 mV, the current sign is negative in the nanocolumn region. In contrast, at voltage >26 mV, the current sign becomes positive. This result points to an inner potential in the Hastelloy C276–nanocolumn system of about 26 mV.

Moreover, by stopping the tip scanning, current–voltage (*I–V*) measurements (Figure 6b) were performed on the single nanocolumn and on plain substrate. Ohmic behaviors were observed in both cases,

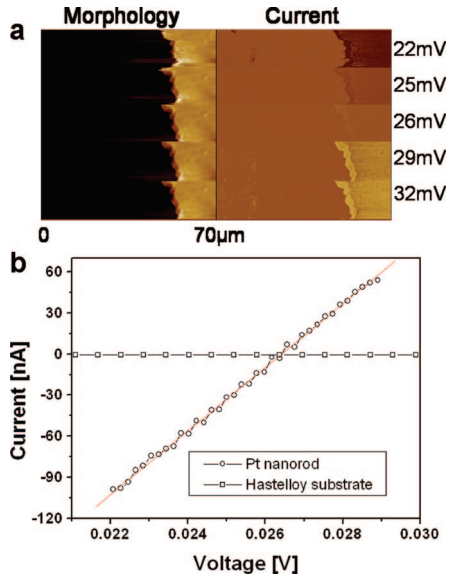

Figure 6. (a) Comparison between the morphological and current imaging at different voltages biased in two regions: covered and not completely covered by nanocolumns. (b) Local current *versus* voltage (*I–V*) plots obtained by stopping the C-AFM scan and performing the electrical measurements on a single nanocolumn and on plain Hastelloy C276 substrate.

and the two patterns cross each other in a singular *I–V* point when the applied voltage is opposed to the inner potential (26 mV). Moreover, the slope of the *I–V* curve was used to calculate the single nanocolumn resistivity from the following relation:

$$\rho = R\frac{A}{l} \quad (1)$$

where R is the resistance calculated on the basis of the C-AFM current measurements, A (70×70 nm^2) is the mean area of a single nanocolumn, and l is the mean length (about 1200 nm).

The evaluated resistivity value is about 22.2×10^{-6} $\Omega \cdot$ cm, only twice the platinum bulk value (10.6×10^{-6} $\Omega \cdot$ cm).

The recorded data indicate that Pt nanocolumns possess very good conductivity. These results demonstrate that there are sufficient mobile charge carriers in the nanodimensional lattice.

DISCUSSION

Nanofabrication aims at building nanoscale structures that can act as components, devices, or systems in large quantity and with potentially low costs. For several decades, MOCVD fabrication has been the most popular industrial synthetic method for the growth of thin films. Here, we show the capabilities and applications of the MOCVD technology for nanofabrication.

The proposed MOCVD approach represents an innovative, low-temperature and low-cost synthetic method that proved to have several advantages over the widely used template and/or catalytic methods for the fabrication of ordered nanostructures.

It is innovative because, to the best of our knowledge, no MOCVD fabrication of nanostructured arrays has been previously reported, besides the growth of epitaxial nanostructure arrays.[52–54] In that case, the growth of the nanostructures was induced by the epitaxial relationship between the nanocolumns and the substrate.

Furthermore, our approach requires mild operational conditions (low deposition temperature and common gasses), and the growth rate is quite high (33.3 nm/min). Moreover, in contrast to the major solu-

tion methods, which cannot produce controlled assemblies of nanocolumns, this method assures the fabrication of uniform ordered arrays on several substrates, including those required in several fields, from catalysis to nanoelectronics, and from biotechnology to gas sensing. As a matter of fact, all these applications require the production of tailored architectures on very large areas.

Finally, and even more importantly, the present approach is absolutely general since it can be adopted for the deposition of fcc materials over any substrate. In fact, the occurrence of the ⟨100⟩ texturing and of the columnary morphology at low deposition temperatures can be rationalized using the growth model reported for metallic and oxide films (Ag, Cu, Al_2O_3, TiO_2) deposited on random substrates by physical vapor deposition (PVD) techniques and by the Mochvan and Demchishin model, respectively.[55,56] Both models rely upon three different kinds of structures and morphologies, depending on the homologous temperature ($T_h = T_{dep}/T_{melting}$).

In particular, polycrystalline or amorphous substrates have irregular atom arrangements on the surface, and there is no definite geometrical similarity between the film and the underlying substrate; thus, under a non-epitaxial growth regime, there is an infinite number of possible orientations and morphologies for growing grains.[55] However, more and more studies on the texture of fcc metals (Ag, Au, Cu, Al, Ni, and Pb) grown on polycrystalline or amorphous substrates have shown that all of them possess predominantly (100) orientation in the 0.3–0.5 T_h range.[55,57]

The PVD growth model related to texturing is based on the differences of surface energies and elastic energies between grains of different orientations.[55,57] For example, in fcc metals, the ⟨111⟩ orientation is favored on the basis of surface energy considerations. Nevertheless, in the 0.3–0.5 homologous temperature range, the ⟨100⟩ texture prevails due to the different elastic energy stored in grains with different orientations. The entire process is, therefore, governed by the balance between differences of the intrinsic elastic stress and the surface energy. The consequence is that grains with lower strain orientation grow at the expense of neighbors having greater strain energy orientations. The increase of the film thickness results in the balancing the bulk and surface energies and causes the predominance of crystallographic planes different than the {111} planes.

Note that the T_h range of the present MOCVD experiments ($0.26 < T_h < 0.34$; $T_{melting}(Pt) = 2045$ K) lies well within the limits reported for PVD processes.

At higher deposition temperatures (450–850 °C), all the present samples are randomly oriented. Temperatures in this range correspond to homologous temperatures in the 0.41–0.5 range, involving crystallite formation controlled by greater surface mobilities. It is reasonable to assume that, under these conditions, surface energies play a more important role in determining the preferred texture, so that ⟨111⟩ orientation is favored.

Therefore, the texture is mainly controlled by the deposition temperature, but it also depends upon the thickness, since grain dimensions control the stored elastic energy while the surface energy is related only to the grain surface. Moreover, we have observed the 111 reflection at film thicknesses >6 μm. These results are in accordance with the proposed model for PVD growth of Ag films, which shows the 111 reflection at film thicknesses >8 μm.

In regard to the morphology, nanocolumns deposited in the $0.27 < T_h < 0.34$ range consist of columnar grains with a length much greater than their lateral dimensions.

In particular, these morphological studies provide further indication that the growth models reported for PVD processes can be extended to the present MOCVD approach and can be rationalized on the basis of the Mochvan–Demchishin zone model.[56]

The validity of the PVD model applied to the present case is corroborated by data collected on different substrates. In any case, Pt nanocolumns grown in identical T ranges show the same morphology, and even in the case of $SrTiO_3$ substrates, which could drive the epitaxial growth of Pt films, only Pt nanocolumns have been observed.

This observation confirms that the present MOCVD process is substrate independent and represents a general approach to grow nanocolums, since in principle it can be applied to fcc materials growing on any kind of substrate.

CONCLUSIONS

The present paper reports on a simple, low-temperature, seedless and template-free MOCVD approach to fabricate oriented Pt nanocolumns. Conductive AFM analysis has been used to measure electrical characteristics at the nanometer scale.

The crystalline quality and orientation of Pt nanocolumns have been carefully controlled by an accurate tuning of operational parameters. There is evidence that morphologies and structures of Pt nanocolumns in the 250–400 °C temperature range do not depend on the nature of substrates, either polycrystalline or oriented, but are strictly determined by operational conditions.

SEM images show that the entire substrate is coated with a highly uniform array of Pt nanocolumns. At $T_{dep} > 400$ °C, platinum random films were obtained on all the investigated substrates.

A suitable rationale for the textural changes *vs* temperature and for the columnar morphology has been related to the zone model already adopted to describe physical vapor deposition processes.

Finally, the electrical response of individual nanocolumns, determined using conductive atomic force microscopy, has shown high conductivity.

EXPERIMENTAL SECTION

The platinum samples were prepared by the MOCVD method using a cold wall horizontal reactor. Bis-acetylacetonate platinum(II) ($Pt(acac)_2$), used as precursor, was purchased from Aldrich Chemicals. It was purified by sublimation at 150 °C and at 10^{-3} Torr before use. The precursor temperature, during standard experiments, was kept constant at 170 °C in order to maintain high vapor pressure and sustain a high deposition rate (33 nm/min). The influence of Pt precursor partial pressure was studied by varying the $Pt(acac)_2$ sublimation temperatures in the 150–180 °C range. Oxygen and argon were used as reaction and carrier gases, respectively. They were introduced through separate lines at 200 sccm O_2 and 100 sccm Ar flow during the standard depositions, and then the oxygen flow was varied in the 50–800 sccm range in order to get oxygen partial pressures of 0.5–8.8 Torr.

Standard experiments were performed using glass as substrate. The glass substrate was mounted onto a stainless steel susceptor with silver paste. The susceptor block was heated with an external ceramic resistance, and the substrate temperature was monitored directly with a thermocouple inserted into the susceptor block. The depositions were performed in the 220–550 °C range for various deposition times (15–360 min). Further experiments were performed on Hastelloy C276 and $SrTiO_3$(100) substrates and gold transmission electron microscope (TEM) grids. Samples grown on the gold grids were used for TEM investigations.

Thicknesses and morphologies were observed for the cross-sectional and surface images using a LEO Iridium 1450 scanning electron microscope (SEM) as well as a JEOL 2010 F TEM. Pt sample purity was determined by WDX analysis using an Oxford Instruments WDX-3PC analyzer. The analyses were carried out at 15 kV accelerating voltage, 10 nA current, and 100 s acquisition time. A thallium acid phthalate (TAP) crystal was used as X-ray selector. X-ray diffraction (XRD) was carried out using a Bruker θ–θ D 5005 diffractometer, working with Cu Kα radiation. Electrical properties were studied by conductive atomic force microscopy (C-AFM). C-AFM measurements were carried out using a conductive tip (boron-doped diamond tips) so that a voltage drop was applied between the conductive tip and the sample. The current amplifier was 100 nA/V. Two operation modes were applied. The conduction current was recorded in the "scanning mode" using a constant voltage. The scan frequency was usually between 0.2 and 0.5 Hz. The applied voltage was negative relative to the sample, and the tip acted as an electron collector. An alternative operation mode involved the use of the tip fixed in a particular location and a sweeping voltage. This configuration represents the nanometric-scale counterpart of microscopic current–voltage measurements. The lateral resolution of our measurements is limited by the tip radius, which is around 10 nm.

Measurements were performed on a Digital Instrument 3100 C-AFM operating in air, in contact mode, and using NANOWORLD diamond-coated boron-doped tips.

Acknowledgment. This work has been partially supported by CNR-INSTM within the PROMO "Nanostrutture organiche, organometalliche polimeriche ed ibride: ingegnerizzazione supramolecolare delle proprietà fotoniche e dispositivistica innovative per optoelettronica" project.

REFERENCES AND NOTES

1. *Handbook of Nanostructured Materials and Nanotechnology*; Nalwa, H. S., Ed.; Academic Press: New York, 2000.
2. *Nanostructured Materials; Clusters, Composites and Thin Films*; Shalaev, V. M., Moskovits, M., Eds.; American Chemical Society: Washington, DC, 1997.
3. *Nanomaterials: Synthesis, Properties and Applications*; Edelstein, A. S., Cammarata R. C., Eds.; Institute of Physics: Philadelphia, PA,1996.
4. Xia, Y.; Yang, P.; Sun, Y.; Wu, Y.; Mayers, B.; Gates, B.; Yin, Y.; Kim, F.; Yan, H. One-Dimensional Nanostructures: Synthesis, Characterization, and Applications. *Adv. Mater.* **2003**, *15*, 353–389.
5. Luryi, S.v; Xu, Y.; Zaslavsky, A. *Future Trends in Microelectronics: The Nanomillenium*; Wiley-Interscience: New York, 2002.
6. Duan, X.; Huang, Y.; Cui, Y.; Wang, J.; Lieber, C. M. Indium Phosphide Nanowires as Building Blocks for Nanoscale Electronic and Optoelectronic Devices. *Nature* **2001**, *409*, 66–69.
7. Björk, M. T.; Ohlsson, B. J.; Thelander, C.; Persson, A. I.; Deppert, K.; Wallenberg, L. R.; Samuelson, L. Nanowire Resonant Tunneling Diodes. *Appl. Phys. Lett.* **2002**, *81*, 4458–4461.
8. Duan, X.; Huang, Y.; Agarwai, R.; Lieber, C. M. Single-Nanowire Electrically Driven Lasers. *Nature* **2003**, *421*, 241–245.
9. Piner, R. D.; Zhu, J.; Xu, F.; Hong, S.; Mirkin, C. A. "Dip-pen" Nanolithography. *Science* **1999**, *283*, 661–663.
10. Tseng, A. A. Recent Developments in Nanofabrication Using Focused Ion Beams. *Small* **2005**, *1*, 924–939.
11. Helt, J. M.; Drain, C. M.; Bazzan, G. Stamping Patterns of Insulating Gold Nanowires with Self-Organized Polymer Films. *J. Am. Chem. Soc.* **2006**, *128*, 9371–9377.
12. Ding, Y.; Mathur, A.; Chen, M.; Erlebacher, J. Epitaxial Casting of Nanotubular Mesoporous Platinum. *Angew. Chem., Int. Ed.* **2005**, *44*, 4002–4006.
13. Kijima, T.; Yoshimura, T.; Uota, M.; Ikeda, T.; Fujikawa, D.; Mouri, S.; Uoyama, S. Noble-Metal Nanotubes (Pt, Pd, Ag) from Lyotropic Mixed-Surfactant Liquid-Crystal Templates. *Angew Chem., Int. Ed.* **2004**, *43*, 228–232.
14. Jiang, X.; Xie, Y.; Lu, J.; Zhu, L.; He, W.; Qian, Y. Simultaneous in-Situ Formation of ZnS Nanowires in a Liquid Crystal Template by γ-Irradation. *Chem. Mater.* **2001**, *13*, 1213–1218.
15. Puntes, V. F.; Krishnan, K. M.; Alivisatos, A. P. Colliodal Nanocrystal Shape and Size Control: the Case of Cobalt. *Science* **2001**, *291*, 2115–2117.
16. Surendran, G.; Apostolescu, G.; Tokumoto, M.; Prouzet, E.; Ramos, L.; Beaunier, P.; Kooyman, P. J.; Etcheberry, A.; Remita, H. From Self-Assembly of Platinum Nanoparticles to Nanostructured Materials. *Small* **2005**, *1*, 964–967.
17. Wyrwa, D.; Beyer, N.; Schmid, G. One-Dimensional Arrangements of Metal Nanoclusters. *Nano Lett.* **2002**, *2*, 419–421.
18. Liu, C. M.; Guo, L.; Wang, R.-M.; Deng, Y.; Xu, H.-B.; Yang, S. Magnetic Nanochains of Metal Formed by Assembly of Small Nanoparticles. *Chem. Commun.* **2004**, 2726–2727.
19. Vivekchand, S. R. C.; Jayakanth, R.; Govindaraj, A; Rao, C. N. R. The Problem of Purifying Single-Walled Carbon Nanotubes. *Small* **2005**, *1*, 920–923.
20. Hwang, C. S.; Lee, B. T.; Kang, C. S.; Kim, J. W.; Lee, K. H.; Cho, H. J.; Horii, H.; Kim, W. D.; Lee, S. I.; Roh, Y. B. A Comparative Study on the Electrical Conduction Mechanisms of $(Ba_{0.5}Sr_{0.5})TiO_3$ Thin Films on Pt and IrO_2 Electrodes. *J. Appl. Phys.* **1998**, *83*, 3703–3713.
21. Goswami, J.; Majhi, P.; Wang, C. G.; Dey, S. K. Properties of Platinum Films by Liquid-Source MOCVD in H_2 and O_2. *Integr. Ferroelectr.* **2002**, *42*, 13–23.

22. Gelfond, N. V.; Galkin, P. S.; Igumenov, I. K.; Morozova, N. B.; Fedotova, N. E.; Zharkova, G. I.; Shubin, Y. V. MO CVD Obtaining Composite coatings from Metal of Platinum Group on Titanium Electrodes. *J. Phys. IV* **2001**, *11*, 593–599.
23. Lux, K. W.; Rodriguez, K. J. Template Synthesis of Arrays of Nano Fuel Cells. *Nano Lett.* **2006**, *6*, 288–295.
24. Choi, K.-S.; McFarland, E. W.; Stucky, G. D. Electrocatalytic Properties of Thin Mesoporous Platinum Films Synthesized Utilizing Potential Controlled Surfactant Assembly. *Adv. Mater.* **2003**, *15*, 2018–2021.
25. Liu, H. T.; He, P.; Li, Z. Y.; Li, J. H. High Surface Area Nanoporous Platinum: Facile Fabrication and Electrocatalytic Activity. *Nanotechnology* **2006**, *17*, 2167–2173.
26. Polli, A. D.; Wagner, T.; Gemming, T.; Rühl, M. Growth of Platinum on TiO_2- and SrO-Terminated $SrTiO_3$(100). *Surf. Sci.* **2000**, *448*, 279–289.
27. Zhou, H.; Wocheer, P.; Schöps, A.; Wagner, T. Investigation of Platinum Films Grown on Sapphire (0001) by Molecular Beam Epitaxy. *J. Cryst. Growth* **2002**, *234*, 561–568.
28. Scavia, G.; Agostinelli, E.; Laureti, S.; Varvaro, G.; Paci, B.; Generosi, A.; Albertini, V. R.; Kaciulis, S.; Mezzi, A. Evolution of the Pt Layer Deposited on MgO(001) by Pulsed Laser Deposition as a Function of the Deposition Parameters: A Scanning Tunneling Microscopy and Energy Dispersive X-ray Diffractometry/Reflectometry Study. *J. Phys. Chem. B* **2006**, *110*, 5529–5536.
29. Francis, A. J.; Cao, Y.; Salvador, P. A. Epitaxial Growth of Cu(100) and Pt(100) Thin Films on Perovskite Substrates. *Thin Solid Films* **2006**, *496*, 317–325.
30. Wang, K.; Yao, K.; Chua, S. J. Titanium Diffusion and Residual Stress of Platinum Thin Films on Ti/SiO_2/Si Substrate. *J. Appl. Phys.* **2005**, *98*, 013538.
31. Zhang, X.; Xie, H. Q.; Fujii, M.; Ago, H.; Takahashi, K.; Ikuta, T.; Abe, H.; Shimizu, T. Thermal and Electrical Conductivity of a Suspended Platinum Nanofilm. *Appl. Phys. Lett.* **2005**, *86*, 171912.
32. Battiston, G. A.; Gerbasi, R.; Rodriguez, A. A Novel Study of the Growth and Resistivity of Nanocrystalline Pt Films Obtained from $Pt(acac)_2$ in the Presence of Oxygen or Water Vapor. *Chem. Vap. Deposition* **2005**, *11*, 130–135.
33. Goswami, J.; Wang, C. G.; Cao, W.; Dey, S. K. MOCVD of Platinum Films from $(CH_3)_3CH_3CpPt$ and $Pt(acac)_2$: Nanostructure, Conformality, and Electrical Resistivity. *Chem. Vap. Deposition* **2003**, *9*, 213–220.
34. Malandrino, G.; Lo Nigro, R.; Fragalà, I. L. MOCVD of Platinum (100) Oriented Films on Random Hastelloy C 276. *Chem. Vap. Deposition* **1999**, *5*, 59–61.
35. Martin, T. P.; Tripp, C. P.; DeSisto, W. J. Composite Platinum/Silicon Dioxide Films Deposited Using CVD. *Chem. Vap. Deposition* **2005**, *11*, 170–174.
36. Puddephatt, R. J. Reactivity and Mechanism in the Chemical Vapor Deposition of Late Transition-Metals. *Polyhedron* **1994**, *13*, 1233–1243.
37. Zinn, A.; Niemer, K.; Kaesz, H. D. Reaction Pathways in Organometallic Chemical Vapor Deposition (OMCVD). *Adv. Mater.* **1992**, *4*, 375–378.
38. Xue, Z. L.; Thridandam, H.; Kaesz, H. D.; Hicks, R. F. Organometallic Chemical Vapor Deposition of Platinum—Reaction-Kinetics and Vapor-Pressures of Precursors. *Chem. Mater.* **1992**, *4*, 162–166.
39. Xue, Z.; Strouse, M. J.; Shuh, D. K.; Knobler, C. B.; Kaesz, H. D.; Hicks, R. F.; Williams, R. S. Characterization of (Methylcyclopentadyenyl) Trimethyl Platinum and Low Temperature Organometallic Chemical Vapor Deposition of Platinum Metal. *J. Am. Chem. Soc.* **1989**, *111*, 8779–8784.
40. Dryden, N. H.; Kumar, R.; Ou, E.; Rashidi, M.; Roy, S.; Norton, P. R.; Puddephatt, R. J.; Scott, J. D. Chemical Vapor Deposition of Platinum—New Precursors and Their Properties. *Chem. Mater.* **1991**, *3*, 677–685.
41. Arndt, J.; Klippe, L.; Stolle, R.; Wahl, G. Deposition of Platinum from Bis(Acetylacetonato) Platinum(II). *J. Phys. IV* **1995**, *5*, C5-114C5-126.
42. Nizard, H.; Gelfond, N. V.; Morozova, N. B.; Igumenov, I. K.; Fietzek, H.; Gimeno-Fabra, L.; Redjaimia, A. Singularity in the Growth of Ptand Ir Films Obtained by Metal-Organic Chemical Vapor Deposition. *Proc. Electrochem. Soc. EUROCVD-15* **2005**, *9*, 754–761.
43. Shin, H. J.; Ryoo, R.; Liu, Z.; Terasaki, O. Template Synthesis of Asymmetrically Mesostructured Platinum Networks. *J. Am. Chem. Soc.* **2001**, *123*, 1246–1247.
44. Liu, Z.; Sakamoto, Y.; Ohsuna, T.; Hiraga, K.; Terasaki, O.; Ko, C. H.; Shin, H. J.; Ryoo, R. TEM Studies of Platinum Nanowires Fabricated in Mesoporous Silica MCM-41. *Angew. Chem., Int. Ed.* **2000**, *39*, 3107–3110.
45. Kyotani, T.; Tsai, L.; Tomita, A. Formation of Platinum Nanorods and Nanoparticles in Uniform Carbon Nanotubes Prepared by a Template Carbonization Method. *Chem. Commun.* **1997**, 701–702.
46. Sakamoto, Y.; Fukuoka, A.; Higuchi, T.; Shimomura, N.; Inagaki, S.; Ichikawa, M. Synthesis of Platinum Nanowires in Organic–Inorganic Mesoporous Silica Templates by Photoreduction: Formation Mechanism and Isolation. *J. Phys. Chem. B* **2004**, *108*, 853–858.
47. Condorelli, G. G.; Malandrino, G.; Fragalà, I. Metal–Organic Chemical Vapor Deposition of Copper and Copper(I) Oxide—Kinetics and Reaction Mechanisms in the Presence of Oxygen. *Chem. Mater.* **1995**, *7*, 2096–2103.
48. Condorelli, G. G.; Malandrino, G.; Fragalà, I. L. Kinetic Study of MOCVD Fabrication of Copper(I) and Copper(II) Oxide Films. *Chem. Vap. Deposition* **1999**, *5*, 21–27.
49. Turgambaeva, A. E.; Krisyuk, V. V.; Bykov, A. F.; Igumenov, I. K. Routes of Metal Oxide Formation from Metal Beta-Diketonates Used as CVD Precursors. *J. Phys. IV* **1999**, *9*, 65–72.
50. Bykov, A. F.; Turgambaeva, A. E.; Igumenov, I. K.; Semyannikov, P. P. Mass-Spectrometric Study of Thermolysis Mechanism of Metal Acetylacetonates Vapor. *J. Phys. IV* **1995**, *C5*, 191–197.
51. Kumar, R.; Roy, S.; Rashidi, M.; Puddephatt, R. J. New Precursors for Chemical Vapor Deposition of Platinum and the Hydrogen Effect on CVD. *Polyhedron* **1989**, *8*, 551–553.
52. Mikkelsen, A.; Sköld, N.; Quattara, L.; Borgström, M.; Andersen, J. N.; Samuelson, L.; Seifert, W.; Lundgren, E. Direct Imaging of the Atomic Structure inside a Nanowire by Scanning Tunneling Microscopy. *Nat. Mater.* **2004**, *3*, 519–523.
53. Johansson, J.; Wacaser, B. A.; Dick, K. A; Seifert, W. Growth Related Aspects of Epitaxial Nanowires. *Nanotechnology* **2006**, *17*, S355–S361.
54. Zhang, B. P.; Binh, N. T.; Wakatsuki, K.; Segawa, Y.; Kashiwaba, Y.; Haga, K. Synthesis and Optical Properties of Single Crystal ZnO Nanorods. *Nanotechnology* **2004**, *15*, S382–S388.
55. *Materials Science in Microelectronics*; Machlin, E. S., Ed.; Gyro: New York, 1995.
56. Mochvan, B. A.; Demchishin, A. V. Structure and Properties of Thick Vacuum-Condensates of Nickel, Titanium, Tungsten, Aluminum Oxide, and Zirconium Dioxide. *Phys. Met. Metallorg.* **1969**, *28*, 653–660.
57. Grantcharova, E.; Dovreb, D. Microstructure and Texture Formation in Vacuum Deposited Silver Films. *Cryst. Res. Technol.* **1993**, *28*, 877–880.